

Laser Cooling of Traveling-Wave Phonons in an Optical Fiber

Joel N. Johnson,^{1,2} Danielle R. Haverkamp^{1D},^{1,2} Yi-Hsin Ou,³ Khanh Kieu,³ Nils T. Otterstrom,⁴ Peter T. Rakich^{5D},⁵ and Ryan O. Behunin^{1,2,*}

¹*Department of Applied Physics and Materials Science, Northern Arizona University, Flagstaff, Arizona 86011, USA*

²*Center for Materials Interfaces in Research and Applications, Flagstaff, Arizona, USA*

³*College of Optical Sciences, University of Arizona, Tucson, Arizona, USA*

⁴*Photonic and Phononic Microsystems, Sandia National Laboratories, Albuquerque, New Mexico, USA*

⁵*Department of Applied Physics, Yale University, New Haven, Connecticut, USA*



(Received 22 May 2023; revised 26 July 2023; accepted 22 August 2023; published 20 September 2023)

In recent years, optical control of mechanical oscillators has emerged as a critical tool for everything from information processing to laser cooling. While traditional forms of optomechanical cooling utilize systems comprising discrete optical and mechanical modes, it has recently been shown that cooling can be achieved in a chip-based system that possesses a continuum of modes. Through Brillouin-mediated phonon-photon interactions, cooling of a band of traveling acoustic waves can occur when anti-Stokes scattered photons exit the system more rapidly than the relaxation rate of the mechanical waves, to a degree determined by the acousto-optic coupling. Here, we demonstrate that a continuum of traveling-wave phonons can be cooled within an optical fiber, extending this physics to macroscopic length scales. Leveraging the large acousto-optic coupling permitted within a liquid-core optical fiber, heterodyne spectroscopy reveals power-dependent changes in spontaneous-Brillouin-scattering spectra that indicate a reduction of the thermal phonon population by 21 K using 120 mW of injected laser power. These results provide alternative ways to manipulate phonon populations that could enable acousto-optic applications with reduced noise or provide ways to control traveling-wave phonons at the quantum level.

DOI: 10.1103/PhysRevApplied.20.034047

I. INTRODUCTION

Laser cooling has brought about a revolution in atomic, molecular, and optical (AMO) physics, permitting exquisite control of the motion of ions, atoms, and molecules, precision measurements of time, and the creation of new states of matter [1–9]. Beyond these applications in AMO physics, laser cooling has led to impressive developments in solid-state systems, where optical refrigeration in rare-earth-doped glasses is rapidly approaching cryogenic operation, and sideband cooling of individual mesoscopic mechanical oscillators has opened windows onto the foundations of physics and enabled the generation of exotic quantum states [10–13].

Laser cooling of mechanical oscillators conventionally utilizes an optical cavity with a movable mirror, where radiation pressure mediates a parametric coupling between a cavity resonance and a discrete phononic mode [13]. This configuration is critical for optical-sideband cooling, where drive-laser photons, with frequencies red-detuned from an optical resonance, can be preferentially blueshifted

by phonon scattering, rapidly exit the system, and lower the effective phonon occupancy [13]. While optomechanical cooling of traveling-wave phonons has been achieved in whispering-gallery-mode resonators that support discrete optical and mechanical modes [14], surprisingly, this form of anti-Stokes cooling can occur in continuous systems, without optical or mechanical resonances [15]. Otterstrom *et al.* [15] showed that cooling of a continuous band of phonon modes can be achieved when injected laser light is scattered through an anti-Stokes process from traveling-wave phonons and exits the system more rapidly than the phonon bath returns to thermal equilibrium. Because distinct traveling phonon modes mediate Stokes and anti-Stokes scattering in a continuous system, it is possible to cool a selected band of phonons, as any simultaneous Stokes “heating” will change the population of a distinct mode. This form of cooling simultaneously requires substantial light-sound coupling, to enable efficient scattering, and phonon lifetimes exceeding the transit time for light through the waveguide. Owing to these stringent requirements, optomechanical cooling in continuous systems has been observed only in silicon waveguides engineered to have a large Brillouin coupling, with a

*ryan.behunin@nau.edu

short length of approximately 1 cm. While the realization of this physics in optical fibers may be attractive for low-noise signal processing, high-coherence lasers, high-fidelity optical squeezing, and variable-bandwidth forms of all-optical slow-light generation, the demonstration of cooling of traveling-wave phonons in fibers has remained elusive [16–18].

Here, we demonstrate cooling of a continuum of phonon modes in an optical fiber. Through spontaneous Brillouin scattering in a 1-m-long CS_2 -filled liquid-core optical fiber, we achieve cooling (i.e., a change in temperature) of approximately 21 K from room temperature for a band of anti-Stokes phonons. This dynamics is made possible by the unique features of this fiber system (Fig. 1) [19–21]. The large refractive index and small sound speed of CS_2 enable guidance and tight coconfinement of light and sound simultaneously [Figs. 1(c) and 1(d)] within small-diameter silica capillaries. This tight acousto-optic overlap, combined with the large electrostrictive coupling made possible in CS_2 [22], permits large light-sound interactions, which can be leveraged for optomechanical cooling in a continuous system.

Using heterodyne spectroscopy, we show how spectra of spontaneously scattered light evolve with the pump power. These spectra reveal signatures of cooling, showing changes in the phonon dissipation rate and a nonlinear dependence on the pump power. To confirm the depletion of thermal phonons, we perform a form of pump-probe spontaneous Brillouin scattering where changes in the phonon population can be directly probed. This pump-probe technique leverages a unique property of Brillouin scattering, permitting two orthogonal polarizations of light

to couple to the same band of phonons. Using this feature, an intense pump can be used to cool the phonon modes while a weak probe laser, in an orthogonal polarization that can be isolated from the pump, measures the phonon population. With a fixed probe power, these results show that the power of the anti-Stokes scattered probe light decreases as the pump power is increased, indicating that the thermal population of the anti-Stokes phonons is reduced in a manner consistent with theory. With the long lengths and power-handling capabilities of optical fibers, combined with recent theoretical developments, these results may enable alternative low-noise fiber applications, ground-state cooling of bands of traveling phonon modes, and alternative forms of quantum state synthesis [23,24].

II. LASER COOLING OF TRAVELING-WAVE PHONONS

Laser cooling of traveling-wave phonons occurs through anti-Stokes Brillouin scattering. During this process, an incident pump photon annihilates a counterpropagating phonon, is blueshifted to higher energy, and rapidly exits the system [Fig. 1(a)]. The frequencies and wave vectors of the participating guided waves satisfy the following phase-matching conditions:

$$\omega_p + \Omega = \omega_{aS}, \quad (1)$$

$$k_p - q = -k_{aS}, \quad (2)$$

where the angular frequencies (wave vectors) of the pump, phonon, and anti-Stokes modes are given by ω_p , Ω , and ω_{aS} (k_p , $-q$, and $-k_{aS}$), respectively. Here, the propagation

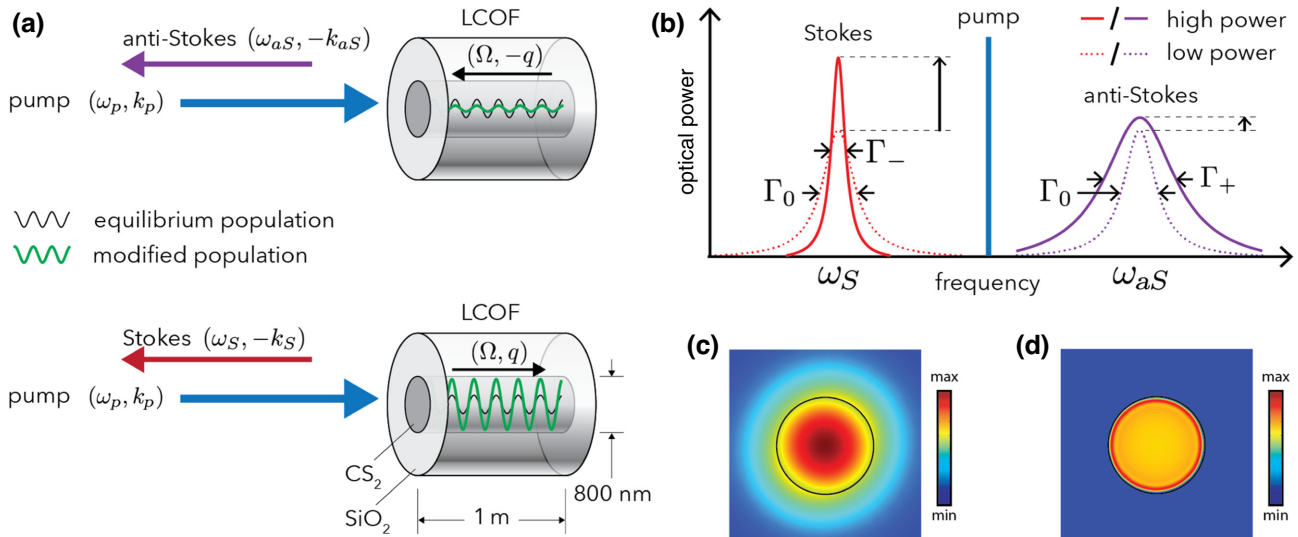


FIG. 1. Illustration of (a) geometry of and scattering processes in a liquid-core optical fiber (LCOF), (b) cooling signatures in spontaneous-light-scattering spectra, and simulated (c) optical and (d) mechanical modes. The simulations in (c),(d) plot the magnitudes of the electric and displacement fields, respectively.

direction of the mode is denoted by the sign of the wave vector. For a selected pump frequency, the dispersion relations for both light and mechanical waves, and Eqs. (1) and (2) can be used to find the frequency of the traveling-wave phonons that participate in anti-Stokes Brillouin scattering,

$$\Omega \approx \frac{2nv}{c} \omega_p, \quad (3)$$

where n is the refractive index, v is the speed of sound, and c is the speed of light in vacuum. It is important to note that Stokes scattering will also occur within the system, tending to increase the population of phased-matched phonons that copropagate with the pump [Fig. 1(a)]. As a result, “heating” of the phonons participating in the Stokes process and cooling of the distinct counterpropagating phonon mode mediating anti-Stokes scattering proceed simultaneously. While cooling of a band of traveling-wave phonons can be achieved and independently detected, unless Stokes scattering is suppressed, the system as a whole will not be cooled.

In order for cooling to occur, the mechanical degrees of freedom must return to thermal equilibrium more slowly than the anti-Stokes photons exit the system. A mean-field analysis of this dynamics, described in Appendix A, shows that these conditions require $4v_g/L > \Gamma_0$, where v_g is the optical group velocity, L is the system length, and Γ_0 is the mechanical dissipation rate [15], conditions met

by the system considered here [Fig. 1(a)] with $4v_g/L \approx 0.82$ GHz and $\Gamma_0 \approx 0.61$ GHz. While the disparate optical and mechanical timescales allow the phonon population to be driven out of thermal equilibrium, the degree of cooling requires a relatively large single-pass Brillouin gain $G \equiv G_B P_p L$, where G_B is the Brillouin gain coefficient [in units of $\text{m}^{-1}\text{W}^{-1}$] and P_p is the pump power [22], yielding a fractional temperature change $\Delta T/T_0$ given approximately by

$$\frac{\Delta T}{T_0} \approx \frac{G}{G + 4}, \quad (4)$$

where T_0 is the equilibrium temperature [15]. Therefore, we must balance competing requirements, maximizing the single-pass gain while minimizing the travel time of light along the fiber, to achieve efficient cooling. Although the mean-field optical decay rate is marginally greater than the phonon decay rate, analysis of the coupled envelope dynamics shows that the key conclusions of the mean-field analysis remain valid in the limit of small single-pass gains explored here (see Sec. A 1).

Cooling of traveling-wave phonons can be identified by power-dependent changes in the width and height of spontaneous-light-scattering spectra, revealing the phonon band temperature and dissipation rate [Fig. 1(b)]. While for low power ($G \ll 1$) the spectrum height increases linearly with the pump power, these increases begin to saturate (grow more rapidly) for the anti-Stokes (Stokes)

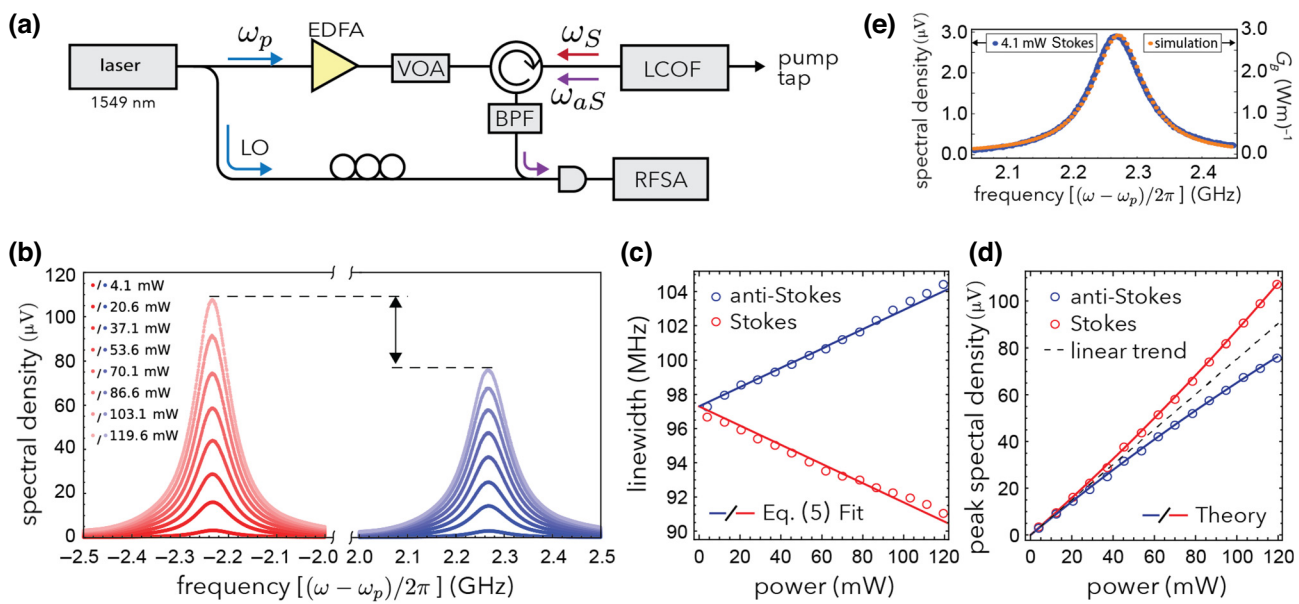


FIG. 2. (a) Heterodyne-spectroscopy apparatus for measuring the power dependence of the spontaneous Brillouin spectra shown in (b). Lorentzian fits to the spectra in (b) reveal signatures of Brillouin cooling through (c) power-dependent linewidths and (d) sublinear and superlinear growth of the peaks in the power spectra. The lines in (c) are obtained through a constrained fit using Eq. (5), providing an estimated Brillouin gain of $2.3 (\text{W m})^{-1}$. The theoretical curves in (d) are obtained using the fitted value of G_B , Eq. (6), and the measured spectrum heights at 4.1 mW (see Appendix A). (e) Comparison between measured and simulated light-scattering spectra (see Appendix C). EDFA, erbium-doped fiber amplifier; BPF, tunable bandpass filter; VOA, variable optical attenuator.

spectrum as the single-pass gain approaches 1 and the phonon population is depleted (increased). Consequently, the anti-Stokes (Stokes) spectrum height grows sublinearly (superlinearly), depending on both the pump power and the phonon population [Figs. 1(b) and 1(d)]. Owing to the additional decay (amplification) channels opened up by spontaneous anti-Stokes (Stokes) Brillouin scattering, the phonon dissipation rate increases (decreases) with the pump power according to

$$\Gamma_{\pm} \approx \Gamma_0 \left(1 \pm \frac{1}{4} G \right), \quad (5)$$

where the upper sign (+) indicates an increase in the anti-Stokes phonon decay rate and the lower sign (−) quantifies how the Stokes spectrum narrows [15]. Interestingly, the Brillouin nonlinearity increases the group velocity of the anti-Stokes photons [25]. As a result, the conditions for cooling can be met even when the phonon decay rate is increased, i.e., $4v_{g,\text{eff}}/L > \Gamma_{+}$ (see Appendix A). As a consequence of these altered decay

rates, the detailed balance for thermal equilibrium is broken, reducing (increasing) the effective population of the anti-Stokes (Stokes) phonons n_{eff}^+ (n_{eff}^-), described by

$$n_{\text{eff}}^{\pm} \approx \frac{\Gamma_0}{\Gamma_{\pm}} n_{\text{th}}, \quad (6)$$

where $n_{\text{th}} \approx 2700$, given by the Bose distribution, is the occupation number for the relevant phonons in our liquid-core optical fiber in thermal equilibrium [15]. See Appendix A for more details of the mean-field analysis of the nonlinear optics in this system.

To demonstrate this physics, we utilize a 1-m-long CS₂-filled silica capillary (Fig. 1), possessing an array of properties that are ideal for laser cooling of traveling-wave phonons. The materials properties and geometry of this liquid-filled capillary permit guided optical (single-mode at 1.55 μm) [Fig. 1(c)] and acoustic waves [Fig. 1(d)] within the 800-nm-diameter fiber core and enable a large Brillouin gain (see Table I in Appendix C for more details). Furthermore, macroscopic meter-scale lengths make large

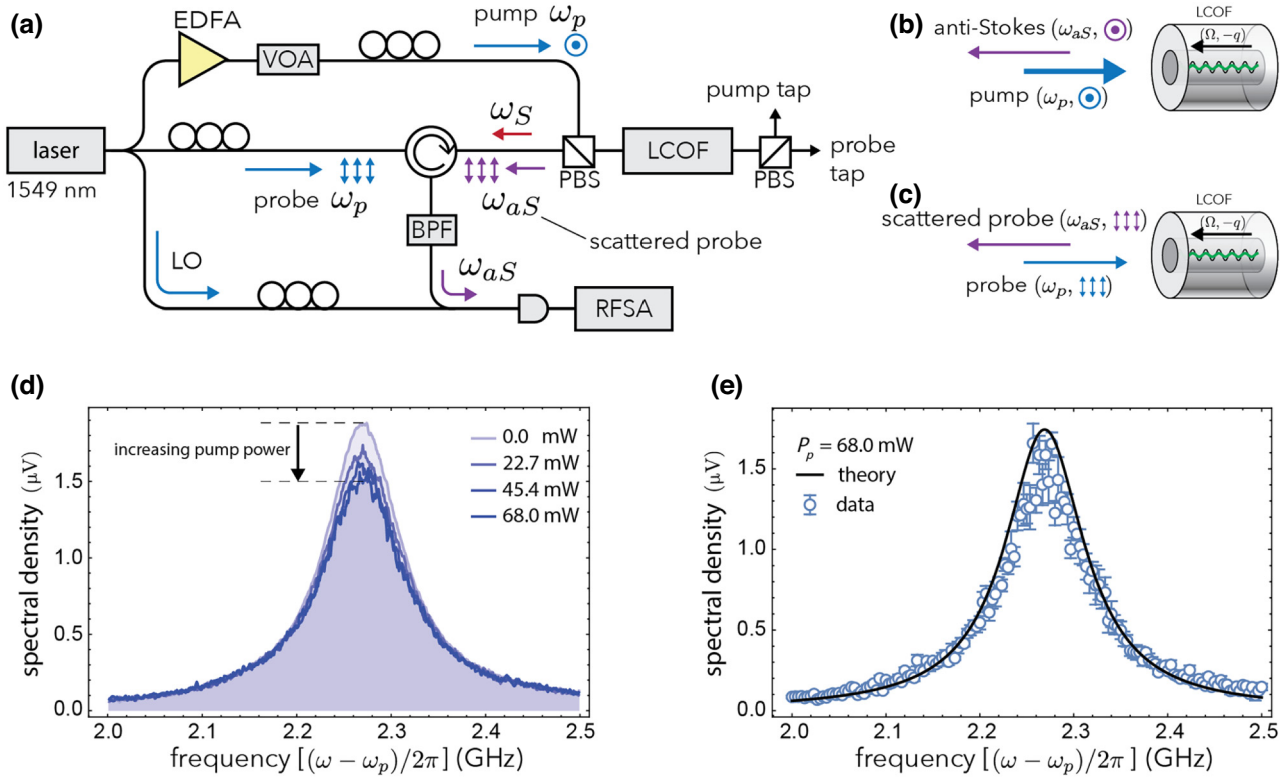


FIG. 3. Pump-probe measurements of Brillouin cooling. (a) Pump-probe spectrometer. Orthogonally polarized pump light and fixed-power probe light are combined and sent into the sample using a polarizing beam splitter (PBS). The backscattered pump and probe light exit from distinct ports of the PBS, and the anti-Stokes sideband is isolated using a circulator and a tunable bandpass filter (BPF). (b),(c) The orthogonally polarized pump and probe beams couple to the same band of phonons. The scattered probe can be isolated from the scattered pump using a PBS. (d) Backscattered anti-Stokes power spectra for the probe, plotted for various pump powers. For clarity, the data are averaged over 1.67-MHz bins. (e) Comparison of measured anti-Stokes spectra and the power spectrum predicted by mean-field theory (see Appendix B).

single-pass gains accessible at modest subwatt powers. See Refs. [19–21] for details of Brillouin scattering in LCOFs.

III. METHODS AND RESULTS

We measure Brillouin cooling in our LCOF using the apparatus shown in Fig. 2(a). The output of a laser is split in two, a variable-power arm is injected into the sample for Brillouin cooling, and a fixed-power arm is used to synthesize a local oscillator (LO) for heterodyne detection. Spontaneously backscattered light is filtered to remove stray pump light and isolate the anti-Stokes (or Stokes) sideband, photomixed with the LO on a high-speed receiver, and detected on a radio-frequency spectrum analyzer (RFSA) as a function of pump power. These measurements yield spontaneous-Brillouin-scattering spectra of the type shown in Fig. 2(b).

The data displayed in Fig. 2 exhibit key signatures of Brillouin cooling. With increasing pump power, the linewidth of the anti-Stokes spectrum increases, and the scattered anti-Stokes power increases sublinearly [Figs. 2(c) and 2(d)]. The extracted linewidths of the Stokes and anti-Stokes spectra exhibit the power dependence described by Eq. (5), yielding a Brillouin gain coefficient $G_B \sim 2.3 (\text{W m})^{-1}$, qualitatively described by the finite-element simulations shown in Fig. 2(e), predicting $G_B \approx 2.9 (\text{W m})^{-1}$. Using Eq. (4), these measurements show that the temperature of the band of traveling anti-Stokes phonons is reduced by 21 K from room temperature with 120 mW of pump power.

The apparatus and data shown in Fig. 2 directly demonstrate the signatures of laser cooling of a continuous band of phonons. However, in these measurements, the amplitude of the power spectrum is proportional to the product of the phonon population and the pump power. To directly detect changes in the phonon population, we utilize the form of pump-probe spectroscopy shown in Fig. 3. In contrast to the heterodyne measurements depicted in Fig. 2, the output of a laser is divided into a variable-power pump and a fixed-power probe. Orthogonally polarized pump and probe beams are combined using a polarizing beam splitter and sent into the LCOF, where they interact with the same phonon mode [Figs. 3(b) and 3(c)]. Owing to this polarization multiplexing, spontaneously backscattered probe light can be separated from the backscattered pump by the PBS, and it is then filtered and photomixed with the LO for heterodyne detection, yielding the spectra shown in Fig. 3(d). In a manner consistent with the depopulation of phonons, these results show a decrease in the anti-Stokes scattering rate with increasing pump power. Furthermore, Fig. 3(c) shows that these spectra are well described by a simple model of pump-probe dynamics, with parameters obtained from the independent measurements shown in Fig. 2. See Appendix B for further details of the pump-probe theory.

IV. CONCLUSIONS

We demonstrate laser cooling of traveling-wave phonons in an optical fiber. Using spontaneous-Brillouin-light-scattering spectroscopy of a CS_2 -filled LCOF, we probe the populations of traveling-wave phonons, revealing power-dependent changes in the phonon dynamics consistent with a mean-field model and finite-element simulations. Key to accessing this regime of light-matter interactions is the large acousto-optic coupling in and short length of our sample, where pump photons readily scatter from counterpropagating phonons and rapidly exit the fiber before the phonons can return to thermal equilibrium. The combination of these properties enables 21 K of phonon cooling with 120 mW of pump power.

Building on these results, drastic enhancements in our ability to cool traveling-wave phonons may be achievable with changes in the fiber geometry and material. With larger core diameters, the Brillouin gain can be dramatically increased through improved acousto-optic overlap as well as through increased optical intensity. Working toward the limit of single-mode operation (for 1.55- μm optical wavelengths), finite-element simulations predict Brillouin gains of approximately $11 (\text{W m})^{-1}$ for an LCOF with a 1.6- μm core diameter, exceeding the acousto-optic coupling in our LCOF by nearly a factor of 5. Under the same experimental conditions as in this study, such a fiber could achieve 119 K of cooling with 250 mW of pump power, approaching cryogenic temperatures. Alternatively, chalcogenide glass fibers can be used to achieve much large Brillouin gains [26]. For example, As_2Se_3 fibers with a 6- μm core diameter can achieve a bulk Brillouin gain $g_B = 6.2 \times 10^{-9} \text{ m/W}$, translating into an approximate Brillouin gain coefficient $G_B \sim 159 (\text{W m})^{-1}$. In such a system, Eq. (4) shows that 100 K of cooling can be achieved in a 1-m fiber with 13 mW of pump power.

As thermal noise produced by traveling-wave phonons is a critical limitation in a variety of fiber-based applications, including information processing, lasers, and quantum optics experiments, these results may inspire alternative ways to achieve improved performance. The techniques demonstrated in this paper may be used to create Brillouin laser technologies with superb stability [27,28], reduce backscatter produced by spontaneous Brillouin scattering in fiber-optic communication, suppress guided-acoustic-wave modulation of quantum optical signals, and enable all-optical delay lines with a tunable bandwidth [18].

ACKNOWLEDGMENTS

J. J. and R. B. acknowledge funding from NSF Award No. 2145724. This article has been authored by an employee of National Technology & Engineering Solutions of Sandia, LLC, under Contract No. DE-NA0003525 with the U.S. Department of Energy (DOE). The employee

owns all right, title, and interest in and to the article and is solely responsible for its contents. The U.S. Government retains, and the publisher, by accepting the article for publication, acknowledges that the U.S. Government retains a nonexclusive, paid-up, irrevocable, worldwide license to publish or reproduce the published form of this article or allow others to do so, for U.S. Government purposes. The DOE will provide public access to these results of federally sponsored research in accordance with the DOE Public Access Plan [32].

APPENDIX A: MEAN-FIELD ANALYSIS OF BRILLOUIN COOLING

The key features of Brillouin cooling can be understood from a mean-field analysis of the slowly-varying-envelope equations. For an undepleted pump and ignoring the propagation of phonons, spontaneous Brillouin scattering can be described by the following coupled stochastic envelope equations:

$$\dot{A}_S + v_g \partial_z A_S = -ig A_p B_S^\dagger, \quad (\text{A1})$$

$$\dot{B}_S + \frac{\Gamma_0}{2} B_S = -ig A_p A_S^\dagger + \xi_S, \quad (\text{A2})$$

$$\dot{A}_{aS} + v_g \partial_z A_{aS} = -ig A_p B_{aS}, \quad (\text{A3})$$

$$\dot{B}_{aS} + \frac{\Gamma_0}{2} B_{aS} = -ig A_{aS} A_p^\dagger + \xi_{aS}, \quad (\text{A4})$$

expressed in a frame rotating at the resonance frequency for each field [29]. Here, A_S (A_{aS}) and B_S (B_{aS}) are the respective right-moving optical and mechanical envelopes for the Stokes (anti-Stokes) process, A_p is the envelope for a constant undepleted pump, g is the Brillouin coupling, and v_g is the optical group velocity. Thermal fluctuations of the mechanical field are modeled using locally correlated white-noise Langevin forces ξ_j ($j = S$ or aS) with correlation properties

$$\langle \xi_j(t, z) \xi_{j'}^\dagger(t', z') \rangle = \Gamma_0(n_{\text{th}} + 1) \delta_{jj'} \delta(t - t') \delta(z - z'), \quad (\text{A5})$$

$$\langle \xi_j^\dagger(t, z) \xi_{j'}(t', z') \rangle = \Gamma_0 n_{\text{th}} \delta_{jj'} \delta(t - t') \delta(z - z'), \quad (\text{A6})$$

where Γ_0 is the mechanical dissipation rate. In terms of readily measurable quantities, the power in an optical mode is given by $P_{S/aS/p} = \hbar \omega_{S/aS/p} v_g A_{S/aS/p}^\dagger A_{S/aS/p}$, and the Brillouin gain can be expressed as

$$G_B = \frac{4|g|^2}{\hbar \omega_p v_g^2 \Gamma_0}. \quad (\text{A7})$$

We define the mean fields for the respective optical and mechanical fields a_j and b_j as the average of the envelope

over the length of the waveguide,

$$a_j = \frac{1}{L} \int_0^L dz A_j(z), \quad (\text{A8})$$

$$b_j = \frac{1}{L} \int_0^L dz B_j(z). \quad (\text{A9})$$

The mean-field equations can be obtained by averaging Eqs. (A1)–(A4) over the waveguide length, giving

$$\dot{a}_S + \frac{\gamma}{2} a_S = -ig A_p b_S^\dagger, \quad (\text{A10})$$

$$\dot{b}_S + \frac{\Gamma_0}{2} b_S = -ig A_p a_S^\dagger + \bar{\xi}_S, \quad (\text{A11})$$

$$\dot{a}_{aS} + \frac{\gamma}{2} a_{aS} = -ig A_p b_{aS}, \quad (\text{A12})$$

$$\dot{b}_{aS} + \frac{\Gamma_0}{2} b_{aS} = -ig a_{aS} A_p^\dagger + \bar{\xi}_{aS}, \quad (\text{A13})$$

where $\bar{\xi}_j$ is the spatial average of the Langevin force. Here, the mean-field optical decay rate $\gamma = 4v_g/L$ is obtained from the spatial average of the derivative terms, assuming $a_j \approx (A_j(L) + A_j(0))/2$ and using the fact that the scattered optical fields vanish at the input face, i.e., $A_j(0) = 0$, according to

$$\begin{aligned} \frac{v_g}{L} \int_0^L dz \partial_z A_k(z) &= \frac{v_g}{L} (A_k(L) - A_k(0)) \\ &= \frac{v_g}{L} (A_k(L) + A_k(0) - 2A_k(0)) \\ &= \frac{2v_g}{L} a_k. \end{aligned} \quad (\text{A14})$$

Next we analyze the mean-field dynamics. When $\gamma > \Gamma_0$, the optical fields respond to changes in the phonon amplitude faster than the phonon changes, enabling a quasistatic solution to the optical-field dynamics given by

$$\frac{\gamma}{2} a_S \approx -ig A_p b_S^\dagger, \quad (\text{A15})$$

$$\frac{\gamma}{2} a_{aS} \approx -ig A_p b_{aS}. \quad (\text{A16})$$

Inserting Eqs. (A15) and (A16) into Eqs. (A11) and (A13), we find that the effective phonon dynamics is given by

$$\dot{b}_S + \frac{1}{2} \Gamma_- b_S = \bar{\xi}_S, \quad (\text{A17})$$

$$\dot{b}_{aS} + \frac{1}{2} \Gamma_+ b_{aS} = \bar{\xi}_{aS}, \quad (\text{A18})$$

where $P_p = \hbar \omega_p v_g A_p^\dagger A_p$, Eq. (A7), and Eq. (2) have been used. In addition to changing the effective phonon dynamics, these results show that the power spectra for the optical

fields are proportional to the phonon power spectrum:

$$S_S[\omega] = \frac{4|g|^2|A_p|^2}{\gamma^2} \int_{-\infty}^{\infty} d\tau e^{i\omega\tau} \langle b_S(t+\tau) b_S^\dagger(t) \rangle, \quad (\text{A19})$$

$$S_{aS}[\omega] = \frac{4|g|^2|A_p|^2}{\gamma^2} \int_{-\infty}^{\infty} d\tau e^{i\omega\tau} \langle b_{aS}^\dagger(t+\tau) b_{aS}(t) \rangle, \quad (\text{A20})$$

illustrating how the optical power spectra, defined by $S_j[\omega] = \int_{-\infty}^{\infty} d\tau \exp\{i\omega\tau\} \langle a_j^\dagger(t+\tau) a_j(t) \rangle$, permit a form of nonequilibrium phonon spectroscopy. Solving Eq. (A17) and using the correlation properties of the spatially averaged Langevin forces given by

$$\langle \bar{\xi}_j(t) \bar{\xi}_{j'}^\dagger(t') \rangle = \frac{1}{L} \Gamma_0 (n_{\text{th}} + 1) \delta_{jj'} \delta(t - t'), \quad (\text{A21})$$

$$\langle \bar{\xi}_j^\dagger(t) \bar{\xi}_{j'}(t') \rangle = \frac{1}{L} \Gamma_0 n_{\text{th}} \delta_{jj'} \delta(t - t'), \quad (\text{A22})$$

we find

$$S_S[\omega] = \frac{\Gamma_0 G}{4v_g} \frac{\Gamma_0 n_{\text{th}}}{\Gamma_-} \frac{\Gamma_-}{\omega^2 + \Gamma_-^2/4}, \quad (\text{A23})$$

$$S_{aS}[\omega] = \frac{\Gamma_0 G}{4v_g} \frac{\Gamma_0 n_{\text{th}}}{\Gamma_+} \frac{\Gamma_+}{\omega^2 + \Gamma_+^2/4}. \quad (\text{A24})$$

The peak of the power spectrum (i.e., on resonance, or at $\omega = 0$), used for the theoretical curves in Fig. 2(e), is given by

$$S_S^{\text{peak}}[P_p] = \frac{n_{\text{th}}}{v_g} \frac{G_B P_p L}{(1 - \frac{1}{4} G_B P_p L)^2}, \quad (\text{A25})$$

$$S_{aS}^{\text{peak}}[P_p] = \frac{n_{\text{th}}}{v_g} \frac{G_B P_p L}{(1 + \frac{1}{4} G_B P_p L)^2}. \quad (\text{A26})$$

To account for the radio-frequency-to-electrical conversion, the peak of the power spectrum at the lowest power ($P_0 = 4.1$ mW) is used to scale the theoretical curves so that they have units of microvolts:

$$S_S^{\text{peak,RF}}[P_p] = \frac{S_S^{\text{peak,RF}}[P_0]}{G_B P_0 L} \frac{G_B P_p L}{(1 - \frac{1}{4} G_B P_p L)^2}, \quad (\text{A27})$$

$$S_{aS}^{\text{peak,RF}}[P_p] = \frac{S_{aS}^{\text{peak,RF}}[P_0]}{G_B P_0 L} \frac{G_B P_p L}{(1 + \frac{1}{4} G_B P_p L)^2}. \quad (\text{A28})$$

1. Envelope analysis of cooling dynamics, and validity of the mean-field model

Here, we show that in the limit of small single-pass gain, the conclusions of the mean-field model agree with the full envelope dynamics.

In the Fourier domain, Eq. (A4) can be readily solved and inserted into Eq. (A3), giving

$$(\partial_z - i\Lambda) A_{aS}(\omega, z) = -\frac{1}{v_g} i g A_p \hat{B}_{aS}(\omega, z), \quad (\text{A29})$$

where

$$\Lambda = \frac{1}{v_g} \left[\omega + i \frac{|g|^2 |A_p|^2}{-i\omega + \Gamma_0/2} \right] \quad (\text{A30})$$

and

$$\hat{B}(\omega, z) = \frac{1}{-i\omega + \Gamma_0/2} \xi(\omega, z). \quad (\text{A31})$$

Using Eqs. (A6) and (A31), the solution to Eq. (A29) at the exit face of the fiber ($z = L$),

$$A_{aS}(\omega, L) = -i \frac{g A_p}{v_g} \int_0^L dz e^{i\Lambda(L-z)} \hat{B}(\omega, z), \quad (\text{A32})$$

can be directly used to obtain the power spectrum of spontaneously scattered anti-Stokes light,

$$\begin{aligned} S_{aS,\text{env}}[\omega] &\equiv \frac{\langle A_{aS}^\dagger(\omega, L) A_{aS}(\omega, L) \rangle}{2\pi\delta(\omega - \omega')} \\ &= \frac{n_{\text{th}}}{v_g} [1 - e^{-G(\omega)}], \end{aligned} \quad (\text{A33})$$

where

$$G(\omega) = \frac{\Gamma_0^2/4}{\omega^2 + \Gamma_0^2/4} G. \quad (\text{A34})$$

Noting that the power spectrum obtained directly from Eq. (A3) is related to the effective phonon power spectrum $S_B[\omega]$,

$$\begin{aligned} S_{aS,\text{env}}[\omega] &= \left| \frac{g A_p}{v_g} \right|^2 \int_0^L dz \int_0^L dz' e^{i(\omega/v_g)(z-z')} \frac{\langle B^\dagger(\omega, z) B(\omega', z') \rangle}{2\pi\delta(\omega - \omega')} \\ &= \left| \frac{g A_p}{v_g} \right|^2 S_B[\omega], \end{aligned} \quad (\text{A35})$$

(note the use of the power spectrum of B as opposed to \hat{B}), we identify the anti-Stokes phonon power spectrum

including the effects of optomechanical cooling,

$$S_B[\omega] = \frac{4n_{\text{th}}L}{G\Gamma_0}(1 - e^{-G(\omega)}). \quad (\text{A36})$$

Using $S_B[\omega]$, we can calculate the effective thermal occupation of the anti-Stokes phonon mode,

$$n_{\text{eff,env}} = \frac{1}{2\pi L} \int_{-\infty}^{\infty} d\omega S_B[\omega] \quad (\text{A37})$$

$$= n_{\text{th}}e^{-G/2}(I_0(G/2) + I_1(G/2)), \quad (\text{A38})$$

where the ω integral can be expressed in terms of the modified Bessel functions I_0 and I_1 . Moreover, the full width at half maximum $\Gamma_{+, \text{env}}$ can be calculated from S_B using $S_B[\Gamma_{+, \text{env}}/2] = S_B[0]/2$, giving the effective anti-Stokes phonon decay rate derived from the envelope dynamics,

$$\Gamma_{+, \text{env}} = \Gamma_0 \left[\frac{G}{-\ln((1 + e^{-G})/2)} - 1 \right]^{1/2}. \quad (\text{A39})$$

In the limit of small single-pass gain G , these results can be compared with the mean-field model, showing agreement to order G for the effective phonon decay rate and to order G^2 for the effective thermal occupation:

$$n_{\text{eff}} \approx n_{\text{th}}(1 - G/4 + G^2/16 - G^3/64 + \dots), \quad (\text{A40})$$

$$n_{\text{eff,env}} \approx n_{\text{th}}(1 - G/4 + G^2/16 - 5G^3/384 + \dots), \quad (\text{A41})$$

$$\Gamma_+ = \Gamma_0(1 + G/4), \quad (\text{A42})$$

$$\Gamma_{+, \text{env}} \approx \Gamma_0(1 + G/4 + G^2/32 + \dots). \quad (\text{A43})$$

For the maximum single-pass gain explored in this study, $G < 0.3$, the results of the mean-field and envelope models agree to better than 0.25% in the effective linewidths and better than 0.007% in the effective thermal occupation. The analysis is similar for the Stokes process.

2. Separation of timescales required for cooling of traveling-wave phonons

For cooling of traveling-wave phonons to occur, anti-Stokes photons must exit the system more rapidly than it takes for the phonons to return to equilibrium, i.e., $4v_g/L > \Gamma_0$. While the optomechanical cooling dynamics leads to an increase in the phonon relaxation rate Γ_+ with pump power, as described by Eq. (5), we can show that a simultaneous increase in the anti-Stokes photon group velocity preserves the required separation of timescales. Noting that the effective anti-Stokes group velocity is

given by

$$v_{g, \text{eff}} = \left(\frac{\partial \text{Re}[\Lambda]}{\partial \omega} \right)^{-1} \approx \left(\frac{1}{v_g} - \frac{G_B P_p}{\Gamma_0} \right)^{-1}, \quad (\text{A44})$$

where Λ is defined in Eq. (A30) and it is assumed that ω is near resonance, i.e., $\omega \ll \Gamma_0$ [18,25], we find that

$$\frac{4v_{g, \text{eff}}}{L} = \frac{4v_g/L}{1 - \frac{1}{4}((4v_g/L)/\Gamma_0)G} > \Gamma_+ = \Gamma_0(1 + G/4). \quad (\text{A45})$$

This result shows that even with the changes in the phonon decay rate produced by the cooling dynamics, the requisite separation of timescales is still satisfied, because the Brillouin nonlinearity produces a fast light effect for the participating anti-Stokes photons.

APPENDIX B: PUMP-PROBE THEORY

In this section, we develop a mean-field theory to describe the pump-probe measurements. In these measurements, both the pump and the probe couple to the same phonon, yielding coupled envelope equations given by

$$\dot{a}_{AS} + \frac{\gamma}{2}a_{AS} = -igA_p b_{AS}, \quad (\text{B1})$$

$$\dot{a}_{\text{sig}} + \frac{\gamma}{2}a_{\text{sig}} = -igA_{\text{pr}} b_{AS}, \quad (\text{B2})$$

$$\dot{b}_{AS} + \frac{\Gamma_0}{2}b_{AS} = -iga_{AS}A_p^\dagger - iga_{\text{sig}}A_{\text{pr}}^\dagger + \bar{\xi}_{AS}, \quad (\text{B3})$$

where A_{AS} is the anti-Stokes light scattered from the pump A_p , and A_{sig} is the anti-Stokes light scattered by the probe, the undepleted probe laser light A_{pr} .

In the quasistatic limit (i.e., $\gamma > \Gamma_0$) and assuming that $|A_p| \gg |A_{\text{pr}}|$, the effective phonon dynamics is given by Eq. (A18), and the power spectrum of the scattered probe light is given by

$$\begin{aligned} S_{\text{sig}}[\omega, P_p] &\equiv \int_{-\infty}^{\infty} d\tau e^{i\omega\tau} \langle a_{\text{sig}}^\dagger(t + \tau) a_{\text{sig}}(t) \rangle \\ &= \frac{\Gamma_0 G_p L P_{\text{pr}}}{4v_g} \frac{\Gamma_0 n_{\text{th}}}{\Gamma_+} \frac{\Gamma_+}{\omega^2 + \Gamma_+^2/4}, \end{aligned} \quad (\text{B4})$$

where P_{pr} is the fixed probe power, and Γ_+ is the phonon decay rate, dependent upon the pump power defined in Eq. (2). This result shows that as Γ_+ increases, i.e., with increasing pump power, the power spectrum broadens and decreases in magnitude. To obtain the theoretical curves shown in Fig. 2(c), we use the peak value of $S_{\text{sig}}[0, 0]$ to determine the constant prefactor in Eq. (B4), where $\Gamma_+ \rightarrow$

Γ_0 , including the optical-to-radio-frequency conversion

$$S_{\text{sig}}[0, 0] = \frac{G_p L P_{\text{pr}}}{v_g} \frac{n_{\text{th}}}{\Gamma_0^2}. \quad (\text{B5})$$

Moving out of the rotating frame yields the prediction for the scattered-probe power spectrum,

$$S_{\text{sig}}^{\text{RF}}[\omega, P_p] = \frac{\Gamma_0^2/4}{(\omega - \omega_{\text{pr}} - \Omega)^2 + \Gamma_+^2/4} S_{\text{sig}}^{\text{RF}}[0, 0], \quad (\text{B6})$$

and this is used to plot the theoretical curves in Fig. 2(e).

APPENDIX C: BRILLOUIN-GAIN SIMULATIONS

We calculate the Brillouin-gain spectrum by utilizing finite-element simulations of the optical and acoustic modes of the LCOF. When empirically derived material properties (see Table I) and damping for silica [30] and CS₂ [31] are included, these simulations yield spatial mode profiles for the electric field **E** and the elastic displacement **u** [Figs. 1(c) and 1(d)]. We obtain the Brillouin gain by evaluating the dissipated mechanical power using the equation

$$G_B = \frac{\omega_p}{\Omega} \frac{1}{P_p P_S} \int_{\text{wg}} d^2x \langle \mathbf{f} \cdot \dot{\mathbf{u}} \rangle, \quad (\text{C1})$$

where P_p and P_S are the pump and Stokes powers, respectively, of the simulated electromagnetic fields, Ω is the angular frequency of the mechanical mode, **f** is the electrostrictive force density, \int_{wg} is an integral over the waveguide cross section, and $\langle \mathbf{A} \cdot \mathbf{B} \rangle$ is the time average of the vector product $\mathbf{A} \cdot \mathbf{B}$. For propagation along the z axis, the

TABLE I. Parameters used in simulations of spontaneous-Brillouin-scattering spectra.

Material	Parameter	Value
CS ₂	Density	1260 kg/m ³
	Refractive index	1.5885
	Speed of sound	1226 m/s
	Electrostrictive constant (γ_e)	2.297
	Acoustic quality factor	23.5
SiO ₂	Density	2203 kg/m ³
	Refractive index	1.445
	Young's modulus	73.1 GPa
	Shear modulus	31.24 GPa
	Photoelastic tensor (p_{11} , p_{12} , p_{44})	(0.125, 0.27, -0.073)
	Acoustic quality factor	1800

electrostrictive force density **f** is given by

$$f_j = \frac{1}{2} \varepsilon_0 n^4 p_{ijkl} \partial_i(E_k E_l^*) \quad (\text{silica}), \quad (\text{C2})$$

$$\mathbf{f} = -\frac{1}{4} \varepsilon_0 \gamma_e \nabla |\mathbf{E}|^2 \quad (\text{CS}_2), \quad (\text{C3})$$

where ε_0 is the permittivity of the vacuum, n is the refractive index, p_{ijkl} is the photoelastic tensor, γ_e is the electrostrictive constant, and the Einstein summation convention is assumed for repeated indices. In these expressions, we neglect the modal differences between the pump and the Stokes fields.

Acoustic dissipation critically determines the predicted power spectrum. We account for dissipation by including empirically obtained acoustic quality factors for silica and CS₂ in our simulations [30,31]. The parameters used in our simulation are summarized in Table I.

- [1] Theodor W. Hänsch and Arthur L. Schawlow, Cooling of gases by laser radiation, *Opt. Commun.* **13**, 68 (1975).
- [2] Arthur Ashkin, Trapping of Atoms by Resonance Radiation Pressure, *Phys. Rev. Lett.* **40**, 729 (1978).
- [3] David J. Wineland, Robert E. Drullinger, and Fred L. Walls, Radiation-Pressure Cooling of Bound Resonant Absorbers, *Phys. Rev. Lett.* **40**, 1639 (1978).
- [4] William D. Phillips and Harold Metcalf, Laser Deceleration of an Atomic Beam, *Phys. Rev. Lett.* **48**, 596 (1982).
- [5] Mike H. Anderson, Jason R. Ensher, Michael R. Matthews, Carl E. Wieman, and Eric A. Cornell, Observation of Bose-Einstein condensation in a dilute atomic vapor, *Science* **269**, 198 (1995).
- [6] Kendall B. Davis, M.-O. Mewes, Michael R. Andrews, Nicolaas J. van Druten, Dallin S. Durfee, D. M. Kurn, and Wolfgang Ketterle, Bose-Einstein Condensation in a Gas of Sodium Atoms, *Phys. Rev. Lett.* **75**, 3969 (1995).
- [7] Andrew D. Ludlow, Martin M. Boyd, Jun Ye, Ekkehard Peik, and Piet O. Schmidt, Optical atomic clocks, *Rev. Mod. Phys.* **87**, 637 (2015).
- [8] Richard I. Epstein, Melvin I. Buchwald, Bradley C. Edwards, Timothy R. Gosnell, and Carl E. Mungan, Observation of laser-induced fluorescent cooling of a solid, *Nature* **377**, 500 (1995).
- [9] Mansoor Sheik-Bahae and Richard I. Epstein, Optical refrigeration, *Nat. Photonics* **1**, 693 (2007).
- [10] Jasper Chan, T. P. Alegre, Amir H. Safavi-Naeini, Jeff T. Hill, Alex Krause, Simon Gröblacher, Markus Aspelmeyer, and Oskar Painter, Laser cooling of a nanomechanical oscillator into its quantum ground state, *Nature* **478**, 89 (2011).
- [11] William Marshall, Christoph Simon, Roger Penrose, and Dik Bouwmeester, Towards Quantum Superpositions of a Mirror, *Phys. Rev. Lett.* **91**, 130401 (2003).
- [12] Sungkun Hong, Ralf Riedinger, Igor Marinković, Andreas Wallucks, Sebastian G. Hofer, Richard A. Norte, Markus Aspelmeyer, and Simon Gröblacher, Hanbury Brown and

- Twiss interferometry of single phonons from an optomechanical resonator, *Science* **358**, 203 (2017).
- [13] Markus Aspelmeyer, Tobias J. Kippenberg, and Florian Marquardt, Cavity optomechanics, *Rev. Mod. Phys.* **86**, 1391 (2014).
- [14] Gaurav Bahl, Matthew Tomes, Florian Marquardt, and Tal Carmon, Observation of spontaneous Brillouin cooling, *Nat. Phys.* **8**, 203 (2012).
- [15] Nils T. Otterstrom, Ryan O. Behunin, Eric A. Kittlaus, and Peter T. Rakich, Optomechanical Cooling in a Continuous System, *Phys. Rev. X* **8**, 041034 (2018).
- [16] Heedeuk Shin, Jonathan A. Cox, Robert Jarecki, Andrew Starbuck, Zheng Wang, and Peter T. Rakich, Control of coherent information via on-chip photonic–phononic emitter–receivers, *Nat. Commun.* **6**, 1 (2015).
- [17] R. M. Shelby, M. D. Levenson, D. F. Walls, A. Aspect, and G. J. Milburn, Generation of squeezed states of light with a fiber-optic ring interferometer, *Phys. Rev. A* **33**, 4008 (1986).
- [18] Yoshitomo Okawachi, Matthew S. Bigelow, Jay E. Sharping, Zhaoming Zhu, Aaron Schweinsberg, Daniel J. Gauthier, Robert W. Boyd, and Alexander L. Gaeta, Tunable All-Optical Delays via Brillouin Slow Light in an Optical Fiber, *Phys. Rev. Lett.* **94**, 153902 (2005).
- [19] K. Kieu, D. Churin, L. Schneebeli, Robert A. Norwood, and N. Peyghambarian, Brillouin lasing in integrated liquid-core optical fibers, *Opt. Lett.* **38**, 543 (2013).
- [20] K. Kieu, D. Churin, E. M. Wright, R. A. Norwood, and N. Peyghambarian, Nonlinear stimulated Brillouin scattering in a single-mode optical fiber, *ArXiv:1402.7089* (2014).
- [21] Ryan O. Behunin, Yi-Hsin Ou, and Khanh Kieu, Spontaneous forward Brillouin scattering in carbon disulfide, *Phys. Rev. A* **99**, 063826 (2019).
- [22] Robert W. Boyd, *Nonlinear Optics* (Academic Press, San Diego, CA, 2020).
- [23] Changlong Zhu and Birgit Stiller, Dynamic Brillouin cooling for continuous optomechanical systems, *ArXiv:2208.06824* (2022).
- [24] Ryan O. Behunin and Peter T. Rakich, Harnessing nonlinear dynamics for quantum state synthesis of mechanical oscillators in tripartite optomechanics, *Phys. Rev. A* **107**, 023511 (2023).
- [25] Miguel Gonzalez-Herraez, Kwang-Yong Song, and Luc Thévenaz, Optically controlled slow and fast light in optical fibers using stimulated Brillouin scattering, *Appl. Phys. Lett.* **87**, 081113 (2005).
- [26] Kazi S. Abedin, Observation of strong stimulated Brillouin scattering in single-mode As_2Se_3 chalcogenide fiber, *Opt. Express* **13**, 10266 (2005).
- [27] Ryan O. Behunin, Nils T. Otterstrom, Peter T. Rakich, Sarat Gundavarapu, and Daniel J. Blumenthal, Fundamental noise dynamics in cascaded-order Brillouin lasers, *Phys. Rev. A* **98**, 023832 (2018).
- [28] Jiang Li, Hansuek Lee, Tong Chen, and Kerry J. Vahala, Characterization of a high coherence, Brillouin microcavity laser on silicon, *Opt. Express* **20**, 20170 (2012).
- [29] Prashanta Kharel, Ryan O. Behunin, William H. Renninger, and Peter T. Rakich, Noise and dynamics in forward Brillouin interactions, *Phys. Rev. A* **93**, 063806 (2016).
- [30] R. Vacher, J. Pelous, F. Plicque, and A. Zarembowitch, Ultrasonic and Brillouin scattering study of the elastic properties of vitreous silica between 10 and 300 K, *J. Non-Cryst. Solids* **45**, 397 (1981).
- [31] Robert W. Coakley and Robert W. Detenbeck, Brillouin-scattering measurements of the acoustic absorption coefficient in liquid CS_2 , *JOSA* **65**, 6 (1975).
- [32] U.S. Department of Energy, DOE Public Access Plan, <https://www.energy.gov/downloads/doe-public-access-plan>.